

Metal nanofilm in strong ultrafast optical fields

Vadym Apalkov¹ and Mark I. Stockman^{1,2,3}¹*Department of Physics and Astronomy, Georgia State University, Atlanta, Georgia 30303, USA*²*Fakultät für Physik, Ludwig-Maximilians-Universität, Geschwister-Scholl-Platz 1, D-80539 München, Germany*³*Max-Planck-Institut für Quantenoptik, Hans-Kopfermann-Strasse 1, D-85748 Garching, Germany*

(Received 8 September 2012; revised manuscript received 26 October 2013; published 26 December 2013)

We predict that a metal nanofilm subjected to an ultrashort (near-single oscillation) optical pulse of a high field amplitude $\gtrsim 3$ V/Å at normal incidence undergoes an ultrafast (at subcycle times $\lesssim 1$ fs) transition to a state resembling semimetal. Its reflectivity is greatly reduced, while its transmissivity and the optical field inside the metal are greatly increased. Despite the metal being a centrosymmetric medium, the strong pulse causes net charge transfer in the direction determined by the carrier envelope phase (CEP) of the pulse, which is opposite to the direction of the maximum field.

DOI: [10.1103/PhysRevB.88.245438](https://doi.org/10.1103/PhysRevB.88.245438)

PACS number(s): 71.30.+h, 42.65.Re, 71.45.Gm, 73.50.Fq

I. INTRODUCTION

The behavior of solids in strong ultrafast optical fields has recently attracted a great deal of attention.^{1–11} Such fields produce nonperturbative effects on solids, among which are ultrafast optical breakdown,¹ attosecond ionization,^{3,4} metallization of dielectric nanofilms,^{6,9} optical field-effect reversible subfemtosecond currents in dielectrics,¹⁰ and electron tunneling from surfaces.^{2,7,8} For dielectrics, when optical field is applied with frequency $\hbar\omega$ low enough compared with the band gap Δ_{vc} between the valence and conduction bands, mostly adiabatic processes take place such as Wannier-Stark (WS) localization and formation of the WS ladder of levels^{12,13} separated by the Bloch frequency¹⁴ $\omega_B = |e|Fa/\hbar$, where e is electron charge, F is the magnitude of the field, and a is the lattice constant. Only when the field F exceeds the critical field $F_c = \Delta_{vc}/(|e|a) \sim 2.5$ V/Å (for $\Delta \sim 10$ eV and $a \sim 4$ Å), the band gap is overcome by the WS splitting, and the diabatic coupling of the valence and conduction band becomes strong, which can lead, in particular, to optical breakdown.¹⁰

In contrast, this paper deals with strong optical fields applied to good (plasmonic) metals where there is no band gap at the Fermi surface, and, consequently, no adiabaticity for relatively low fields. In such a case, there are a high optical conductivity and a skin layer with a depth $l_s \sim 25$ nm.¹⁵ Consequently, for metal thickness $h \gtrsim l_s$, most of the incident radiation energy is reflected. Interaction of the radiation with the metal becomes adiabatic only when the optical field is strong enough so $\omega_B \gg \omega$. The plasmonic metal behavior seizes and WS localization^{12,13} is established when, during a quarter optical period $T/4 = \pi/(2\omega)$, an electron acquires momentum $\pi|e|FT/4$ that exceeds the width $2\pi\hbar/a$ of the Brillouin zone. This condition is satisfied and the strong-field regime for the metal sets on when the optical field $F \gtrsim F_c$, where the critical field $F_c \sim 4\hbar\omega/(|e|a) \approx 2.6$ V/Å for $\hbar\omega = 1.55$ eV.

To elaborate in brief, for $F \gtrsim F_c$, the electrons during a quarter optical cycle accelerate to the Brillouin zone boundary, experiencing the Bragg reflections and, consequently, strong dephasing. This seizes the electron translational motion and is the underlying cause of the strong WS localization within length $l_{WS} \lesssim a$ and the Bloch oscillations. The different electron wave packets are all identical in shape and localized

at each unit cell, their spectrum is discrete with energies spaced by $|eF|a = \hbar\omega_B$, forming the so-called WS ladder. Since $\omega_B \gg \omega$, the field-induced adiabaticity sets in, and the dynamics is driven by the *instantaneous* optical field.

As a consequence of the adiabaticity, in this strong-field regime, the optical properties of the metal differ dramatically from those at low to moderate fields, becoming reminiscent of a semimetal. The latter is a solid with a very small or nonexistent band gap between the valence and conduction bands and a negligible density of electronic states at the Fermi level. For the metal in the strong field, the plasmonic properties and strong reflection associated with the skin effect are suppressed during subcycle time intervals. Light transmission through the metal is increased and the optical absorption in the metal is reduced at very high fields. Ultrafast behavior of the metal is radically changed: both the reflection and transmission exhibit subcycle Bloch oscillations with period $\tau_B \sim 2\pi/\omega_B$; $\tau_B \sim 0.7$ fs for $F = 2.6$ V/Å. The strong optical field is predicted to cause ultrafast response of the metal, which adiabatically follows the instantaneous pulse field. Under these conditions, the Bloch oscillations are predicted to manifest themselves in natural metals, while earlier such oscillations were observed only in artificial semiconductor superlattices.^{16–18} These predicted strong-field effects open up routes toward using metals as active elements for deep ultrafast modulation of optical fields in contrast to perturbative modulation in active plasmonics.¹⁹

II. MODEL AND MAIN EQUATIONS

Consider an ultrashort optical pulse incident normally on a metal nanofilm. Propagation of such a pulse is described by the Maxwell equations where dielectric polarization is determined by quantum dynamics of electrons, which is self-consistently determined by the Schrödinger equation in the presence of the electric field inside the metal.

We neglect the short-range Coulomb scattering of electrons, which determines plasmonic relaxation in metals, because its characteristic time τ_s for good plasmonic metals is known to significantly exceed the length of our optical pulse (e.g., $\tau_s = 10$ – 50 fs for gold and silver).¹⁵ This “instantaneous freedom” approximation worked very well describing

field-induced currents and attosecond phenomena in dielectrics in strong ultrafast fields,^{10,11} where the maximum conduction-band electron concentration was, in fact, on the same order as in metals. Note that the long-range Coulomb interaction is taken into account electrostatically through the self-consistent macroscopic electric field inside the metal.

We solved numerically a coupled system of the Maxwell and Schrödinger equations using the finite difference time domain (FDTD) method^{20,21} for a finite-size system with the absorbing boundary conditions for Maxwell equations. The tight-binding model was used in the solution of the Schrödinger equation. The size of the computational space in the direction of propagation of the pulse (z direction) was 6000 nm. The metal film was placed at the midplane of the system, i.e., at $z = 0$. In our numerical solution of the Maxwell equations, we assumed that the spatial step was 1 nm and the time step was 0.7 attoseconds (1 as = 10^{-18} s). The optical pulse was generated at the left boundary and propagated along the positive direction of the z axis with the polarization of the electric field along the x axis.

To avoid optical damage and effects of electron-electron and electron-phonon scattering (dephasing and dissipation), we need as short pulses as possible. We assume a single-oscillation pulse form:

$$F_x(t) = F_0 e^{-u^2} (1 - 2u^2), \quad (1)$$

where F_0 is the amplitude, which is related to power $\mathcal{P} = cF_0^2/4\pi$, where c is speed of light, $u = t/\tau$, and τ is the pulse length, which is set $\tau = 1$ fs in our calculations. Such a pulse possesses zero area, $\Theta = 0$, where $\Theta = \int_{-\infty}^{\infty} F_x(t) dt$. This pulse is an idealization of the pulses that have recently been used in experiments,^{10,11} which can be called “ $1\frac{1}{2}$ -oscillation” pulses, where only the central, high-amplitude oscillation is effective due to the strong nonlinearity of the system.

The metal is described by one-particle Schrödinger equation with Hamiltonian

$$\mathcal{H} = \frac{\mathbf{p}^2}{2m} + V(\mathbf{r}) + eF_x(z,t)x, \quad (2)$$

where $V(\mathbf{r})$ is the periodic crystal potential, and $F_x(z,t)$ is the optical electric field inside the metal, which is found from the solution of the Maxwell equations. Without the optical field, the electron system has the standard band structure. Below, we consider one conduction band (CB, or sp band for silver) and one valence band (VB, or d band for silver).

We assume that the periodic potential $V(\mathbf{r})$ is separable in all three directions, x , y , and z , with period a . Correspondingly, the electron wave functions factorize, and the energies are additive. For each band, the energy dispersion law along one direction, has the tight-binding form.^{22,23} Considering the x direction, $E_\alpha(k) = \epsilon_\alpha + \frac{\Delta_\alpha}{2} \cos(ka)$, where $\alpha = c$ or v for CB and VB, respectively, Δ_α is the width of band α , and ϵ_α is the band offset. In the absence of the optical field, the wave functions satisfy the Bloch theorem, $\psi_{\alpha k}(x) = \frac{1}{2\pi} e^{ikx} u_{\alpha k}(x)$, where $u_{\alpha k}(x+a) = u_{\alpha k}(x)$ are periodic unit-cell Bloch functions, and k is the (pseudo) wave vector.

In the presence of the optical field, $F_x(z,t)$, we solve the time-dependent Schrödinger equation for an infinite crystal to find the polarization (currents) needed for the Maxwell

equations. The finite thickness of the metal nanofilm is taken into account by the Maxwell boundary conditions imposed on the electrodynamic problem at the two surfaces of the metal. Thus we neglect the spatial dispersion of the metal optical response and the surface states at the metal surfaces. Such an approximation is commonly used in metal nanoplasmonics where it is shown to work very well for metal thickness $h \gtrsim l_{nl}$, where nonlocality length $l_{nl} \sim v_F/\omega \sim 1$ nm, and v_F is the Fermi velocity.¹⁵

Capitalizing on the assumed separability of the crystal potential, we solve the time-dependent Schrödinger equation in the x direction of the optical field polarization (the propagation direction of the electromagnetic wave is z). Note that the three-dimensional nature of the crystal is still important to have the correct density of electronic states and electron concentrations in the bands of the crystal. We express the general solution of the Schrödinger equation in the basis of the Bloch functions as

$$\Psi(x,z,t) = \sqrt{\frac{a}{2\pi}} \sum_{\alpha=v,c} \int_{-\pi/a}^{\pi/a} dk \phi_\alpha(k,z,t) \psi_{\alpha k}(x), \quad (3)$$

where $\phi_\alpha(k,z,t)$ can be expressed in term of the Houston functions²⁴ $\Phi_{\alpha q}^{(H)}(k,z,t)$,

$$\phi_\alpha(k,z,t) = \sum_q \hat{\beta}_\alpha(q,z,t) \Phi_{\alpha q}^{(H)}(k,z,t), \quad (4)$$

$$\begin{aligned} \Phi_{\alpha q}^{(H)}(k,z,t) &= \tilde{\delta}(k - k_T(q,t)) \\ &\times \exp\left(-i \left\{ t \frac{\epsilon_\alpha}{\hbar} + \frac{\Delta_\alpha}{2\hbar} \int_{-\infty}^t dt_1 \cos[k_T(q,t_1)a] \right\}\right). \end{aligned} \quad (5)$$

Here, the time-dependent wave vector is defined as

$$k_T(q,t) = q + \frac{e}{\hbar} \int_{-\infty}^t F_x(z,t_1) dt_1 \quad (6)$$

and $\tilde{\delta}(k) = \sum_n \delta(k + 2\pi n/a)$, where $n = 0, \pm 1, \dots$ and $\delta(k)$ is the Dirac δ function. The Houston functions are exact solutions of the time-dependent Schrödinger equation for a single band with the Bloch function $\psi_{\alpha q}(x)$ as the initial condition at $t = -\infty$.

Expansion coefficients $\hat{\beta}_\alpha(q,z,t)$ satisfy the equations

$$\frac{d\hat{\beta}_\alpha(q,z,t)}{dt} = -i \frac{F_x(z,t)}{\hbar} \sum_{\alpha' \neq \alpha} Q_{\alpha\alpha'}(q,z,t) \hat{\beta}_{\alpha'}(q,z,t),$$

where we denoted

$$\begin{aligned} Q_{\alpha\alpha'}(q,z,t) &= Z_{\alpha\alpha'} \exp\left\{ i \left[t \frac{\epsilon_\alpha - \epsilon_{\alpha'}}{\hbar} \right. \right. \\ &\quad \left. \left. + \frac{\Delta_\alpha - \Delta_{\alpha'}}{2\hbar} \int_{-\infty}^t dt_1 \cos\left(q + \frac{ea}{\hbar} \int_{-\infty}^{t_1} F_x(z,t_2) dt_2 \right) \right] \right\}, \\ Z_{\alpha\alpha'} &= \frac{e}{a} \int_{-a}^a dz u_{\alpha k}(z)^* i \frac{\partial}{\partial k} u_{\alpha' k}(z). \end{aligned} \quad (7)$$

Here, $u_{\alpha k}(z)$ are periodic unit-cell Bloch functions, and dipole matrix elements $Z_{\alpha\alpha'}$ describe diabatic coupling of VB and CB in optical field.

The electric current generated by electron dynamics in the optical-pulse electric field has two contributions, interband and intraband, and is expressed as

$$J_x = J_x^{\text{inter}} + J_x^{\text{intra}}. \quad (8)$$

The interband current is

$$J_x^{\text{inter}}(z,t) = \partial P_x^{\text{inter}}(z,t)/\partial t, \quad (9)$$

where $P_x^{\text{inter}}(z,t)$ is the interband polarization, which has the following form:

$$P_x^{\text{inter}}(z,t) = \frac{1}{2\pi a^3} \int_{-\pi}^{\pi} dq \sum_{\mu=v,c} f_{\mu}(q) \times [\mathcal{B}^{(\mu)\dagger}(q,z,t) \hat{Q}(q,z,t) \mathcal{B}^{(\mu)}(q,z,t)], \quad (10)$$

where \hat{Q} is a matrix with elements (7) $Q_{\alpha\alpha'}$, and $\mathcal{B}^{(\mu)} = (\hat{\beta}_v, \hat{\beta}_c)$ is a two-component vector, which is determined by the solution of Eq. (7) with the following initial conditions: $\mathcal{B}^{(v)} = (1,0)$ and $\mathcal{B}^{(c)} = (0,1)$. Here, $f_{\mu}(q)$ is the Fermi factor, which is 1 for initially occupied states, i.e., $f_{\mu=v}(q) = 1$ and $f_{\mu=c}(|q| < k_F) = 1$, where k_F is the Fermi wave vector, and it is zero otherwise. The intraband current is due to shifting of electrons in space and is expressed as

$$J_x^{\text{intra}}(z,t) = \frac{1}{2\pi a^3} \int_{-\pi}^{\pi} dq \sin[k_T(q,t)a] \times \sum_{\mu=v,c} f_{\mu}(q) \left[\sum_{\alpha=v,c} \mathcal{B}_{\alpha}^{(\mu)\dagger}(q,z,t) \frac{\Delta_{\alpha}}{2\hbar} \mathcal{B}_{\alpha}^{(\mu)}(q,z,t) \right]. \quad (11)$$

We use the tight-binding model parameters describing the band structure of silver: $\epsilon_v = -4.1$ eV, $\epsilon_c = 0$ eV, $\Delta_v = 0.82$ eV, and $\Delta_c = -9.1$ eV. We choose $Z_{vc} = 0.7e \text{ \AA}$.²⁵ The thickness of the film is set $h = 25$ nm.

Although the lattice constant of the silver 3D crystal is $a_0 \approx 4.1$ \AA, it does not determine the lattice constant a of the 1D model used in our calculations. The lattice constant of such an effective 1D model is equal to the period of the 3D lattice in the direction of the electric field of the pulse. This period is defined as the distance between the corresponding crystallographic planes normal to the field direction. The 1D periods are achieved along the high-symmetry directions of the crystal. For such directions, we can define the effective lattice constant as $a = \pi/k_s$, where k_s is the wave vector corresponding to a high-symmetry point of the first Brillouin-zone boundary. For the face centered cubic (fcc) crystal of silver, we choose $k_s = \sqrt{3}\pi/a_0$, which corresponds to the L point of the Brillouin zone. The corresponding 1D lattice constant is $a = a_0/\sqrt{3} \approx 2.4$ \AA. This value is used in our calculations.

III. RESULTS AND DISCUSSION

In Fig. 1(a), the spatial distribution of the pulse electric field is shown for the reflected (to the left of the nanofilm) and transmitted (to the right) pulses. For a relatively small

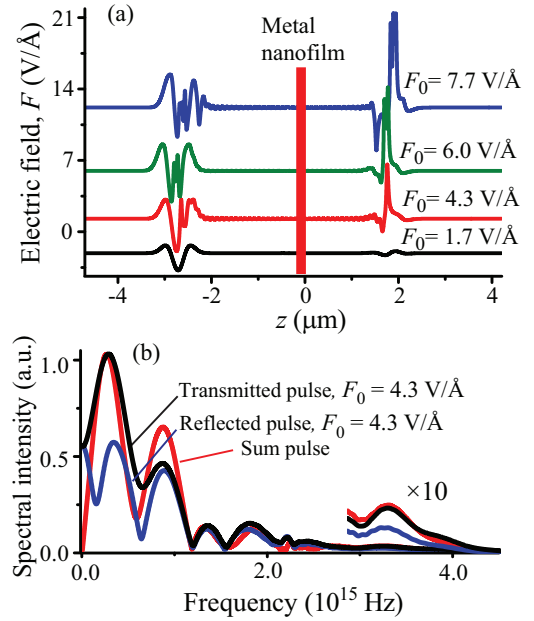


FIG. 1. (Color online) Reflected and transmitted pulses. (a) Spatial distributions of the electric field as functions of the propagation coordinate z shown for different values of F_0 . The metal film of thickness 25 nm is placed at the center ($z = 0$) and depicted as the red stripe. The distribution of electric field consists of the reflected (to the left) and transmitted (to the right) pulses propagating in the opposite directions. The size of the computational field in the z direction is 6000 nm. (b) Spectral intensities of reflected, transmitted, and sum pulses for $F_0 = 7.7 \text{ V/\AA}$ as functions of optical frequency $f = \omega/(2\pi)$. The transmitted- and sum-pulse spectra are arbitrarily normalized to unity maximum. The reflected pulse spectrum is normalized by the same coefficient as the transmitted one. Fragments of the curves at $f > 2$ PHz are also shown with the $\times 10$ magnification as indicated on the graph.

field amplitudes, $F_0 = 1.7 \text{ V/\AA} < F_c$, the nanofilm behaves as a regular metal with a pronounced skin effect and strong reflection of the incident pulse. With increasing the field, $F_0 = 4.3 \text{ V/\AA} \gtrsim F_c$, the response of the electron system is highly nonlinear, and the metal film becomes relatively transparent. Both the reflected and transmitted pulses are strongly reshaped compared to the incident pulse. As the pulse peak field further increased to $F_0 = 6.0$ and 7.7 V/\AA , the film transparency is further increased, in a sharp contrast to the metallic behavior. There are pronounced subperiod oscillations in the pulse shape for both the reflected and transmitted fields, which are due to the Bloch oscillations.

Importantly, in Fig. 1(a), there are nonzero pulse areas, $\Theta^{(t,r)} = \int_{-\infty}^{\infty} F(z^{(t,r)}, t) dt \neq 0$, where t and r correspond to the transmission and reflection, and $z^{(t)} > 0$ and $z^{(r)} < 0$. This is due to nonlinearity of the field interaction with the metal. In contrast, the area of the incident laser pulse of Eq. (1) is exactly zero. When the absorption in the matter is small, which is the case presently, then $|\Theta^{(r)} + \Theta^{(t)}| \ll |\Theta^{(r)}| + |\Theta^{(t)}|$. This implies that the nonlinearity of the metal nanofilm separates the zero-area laser pulse into the transmitted and reflected pulses with the nonzero and approximately opposite areas.

The nonzero area pulses do not contradict Maxwell equations, and fundamentally they can exist. For instance, for an optically-linear uniform medium, a plane wave with fields $E_x = H_y = f(z - tc)$, where f is an arbitrary function, and c is speed of light, is a general solution of the Maxwell equations. Experimentally, near unipolar, half-cycle electromagnetic pulses were generated by aperiodic acceleration of electrons in photoconductive switches in terahertz domain.^{26,27} Such pulses accelerate and transfer momentum and energy to free and quasifree electrons such as those in Rydberg states.^{26,27}

The magnitudes and signs of the predominant fields for both transmission and reflection are determined by carrier-envelope phase φ_{CE} of the excitation pulse, as characteristic for nonlinear effects in a few-oscillation fields, cf. Refs. 10 and 11. Our laser-source pulses possess $\varphi_{CE} = 0$, see Eq. (1), and nonlinearity is such that both absorbance and reflectance decrease with the field (cf. Fig. 3 below); consequently, $\Theta^{(t)} > 0$ and $\Theta^{(r)} < 0$. For $\varphi_{CE} = \pi$, the sign of the dominant field would change to the opposite yielding $\Theta^{(t)} < 0$ and $\Theta^{(r)} > 0$. For $\varphi_{CE} = \pm\pi/2$, both the transmitted and reflected pulses have zero areas.

The present effect can be used to generate near-half-cycle pulses in the near-infrared, visible, and near-ultraviolet spectral regions, in contrast to the previous studies^{26,27} limited to the terahertz band. With regard to this, we need to emphasize two points. (i) Based on a very short pulse duration, our theory does not include relaxation, which on longer times would cause opposite currents and, correspondingly, tend to make the electromagnetic pulses closer to zero-area ones. However, these longer-time currents will generally be not exactly time-reversed with respect to the currents during the pulse due to nonlinearity and frequency dispersion of the metal's optical responses. In particular, these currents will occur without a strong external driving field, unfold on a longer time scale, and be subject to and limited by the dissipation (electron-electron and electron-phonon relaxation). Therefore the nonzero area of the pulses may be expected to persist even after the relaxation. (ii) Due to the presence of low (ideally, zero) frequency components in the spectra of the unidirectional pulses, they will rapidly diffract. Therefore they should be observed and used close to the generating (i.e., irradiated) area of the metal nanofilm, i.e., at distances on the order or less than the size of this area.

In Fig. 1(b), we display spectral intensities of the transmitted and reflected pulses $I^{(t,r)}(f) = |F_f^{(t,r)}|^2$, where subscript f indicates Fourier transform in terms of linear frequency $f = \omega/(2\pi)$. For $f = 0$, $I^{(t,r)}(0) = [\Theta^{(t,r)}]^2 \neq 0$, in accord with the nonzero pulse areas.

Besides peaks at the carrier frequency, $f \approx 0.25$ PHz, in Fig. 1(b) there are peaks approximately at the third harmonic frequency, $f \approx 0.75$ PHz, which are due to the strong nonlinearity. There are also appreciable peaks at the Bloch frequency, $f \approx 3.5$ PHz, which are shown magnified by a factor of $\times 10$. Observation of these peaks, which stem from the Bloch oscillations,^{14,16-18} would be the first evidence of the Bloch oscillations in natural crystals as opposed to the artificial superlattices.

The enhanced transmission of the superstrong optical pulse is accompanied by an increase of the electric field F^{metal} inside the metal nanofilm. In Fig. 2, we show the time

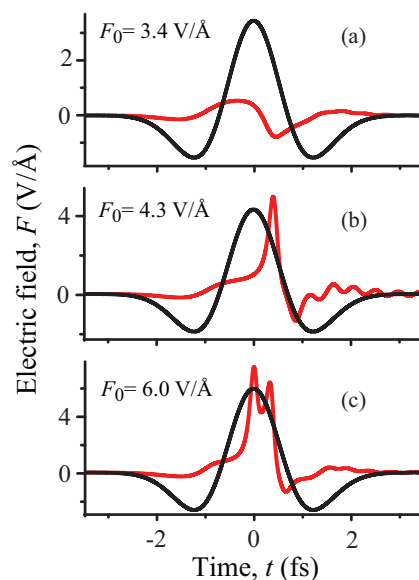


FIG. 2. (Color online) The electric field of the incident pulse (black lines) and the electric field at the midpoint of the metal film (red line) are shown for different values of the peak electric field F_0 of the incident pulse: (a) $F_0 = 3.4$, (b) 4.3, and (c) 6.0 V/Å. Note that the pulse areas are nonzero, cf. discussion of Fig. 1, which causes current and charge transfer along the metal in the x direction.

evolution of this field at the midplane of the nanofilm in comparison to the incident pulse. At a near-critical pulse field $F_0 = 3.4$ V/Å $\sim F_c$, see Fig. 2(a), the electric field F^{metal} inside the metal is much weaker than the incident field. In contrast, for larger pulse amplitudes ($F_0 = 4.3$ and 6.0 V/Å), see Figs. 2(b) and 2(c), the electric field F^{metal} becomes comparable to the incident-pulse electric field. The sharp peaks and high-frequency oscillations of F^{metal} are due to the Bloch oscillations, as we discuss below in conjunction with Fig. 4.

The reflectance of the optical pulse (i.e., a fraction of the reflected pulse energy) is shown in Fig. 3(a) as a function of F_0 . Strong suppression of the pulse reflectance for $F_0 > F_c \sim 3.4$ V/Å is clearly visible. The suppression of the reflectance is correlated with increase of the maximum electric field inside the nanofilm shown by the red line in Fig. 3(a) as $F_{\text{max}}^{\text{metal}}/F_0$. The strong changes in both the reflectance and the internal electric field occur at $F_0 \sim F_c \sim 3.4$ V/Å.

The absorbance of the metal nanofilm, that is, a fraction of the pulse energy dissipated inside the nanofilm, is illustrated in Fig. 3(b) as a function of amplitude F_0 . This predicted behavior is unusual and nontrivial. At a low pulse amplitude, the absorbance is understandably low due to the skin effect since mostly the pulse is reflected back. Then, as F_0 increases, the absorbance increases dramatically reaching $\approx 4\%$ maximum for $F_0 \approx 5$ V/Å, which is attributed to the WS localization leading to the collapse of the metallic conductivity, consequent suppression of the skin effect, and the resulting penetration of the field inside the metal—cf. the red line in panel (a).

With the further increase of F_0 , the absorbance in Fig. 3(b) decreases despite the field in the metal staying almost the same. This is due to two effects. First, for $F \gtrsim F_c$, the spacing

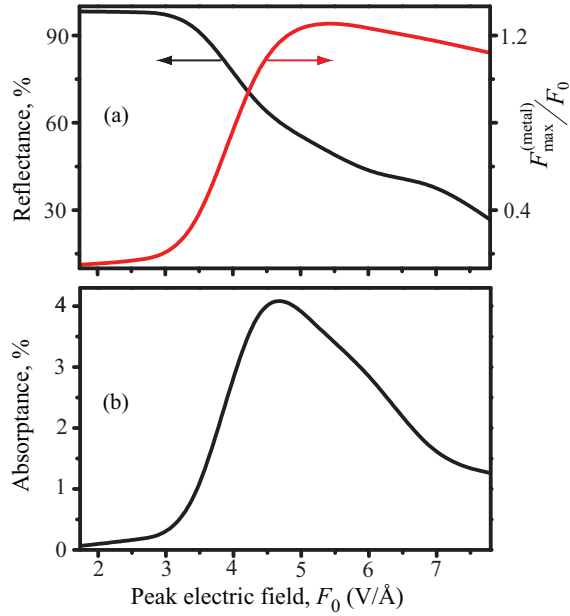


FIG. 3. (Color online) (a) The reflectance of optical pulse (black line) and the maximum electric field at the midpoint of the nanofilm (red line) are shown as functions of the peak electric field F_0 of the incident pulse. The maximum electric field in the metal film is shown in units of the peak electric field F_0 . (b) The absorbance of the optical pulse is shown as a function of the peak electric field F_0 .

between the WS levels increases to yield $\omega_B \gg \omega$. This leads to the adiabaticity of the light-solid interaction, which implies suppression of the absorbance. Second, the Bloch oscillations, which develop for the same field strength (see below Fig. 4 and its discussion), break phase ϕ of the optical polarization with respect to the excitation field and, consequently, reduce the work of this field, which is $\propto \sin \phi$. Effectively, for the high fields, the nanofilm is acquiring properties of a semimetal with a low active conductivity characteristic of semimetals.

The power density dissipated from a single pulse in the metal reaches its maximum also at $F_0 \approx 5$ V/Å. After its dissipation and thermal equilibration, this causes an estimated increase of the nanofilm temperature by ~ 1500 K. The metal may not survive such a high-intensity pulse without a damage; however, this damage will be melting, which occurs long after the pulse is over. This will not prevent the much faster effects described from being observable but will require single-shot experiments. Note that a metal is likely to survive lower-field pulses with $F_0 \sim 2\text{--}3$ V/Å, which explains the absence of optical damage of metal electrodes subjected to comparable pulses in experiments of Ref. 10.

The origin of this highly nonlinear behavior of a metal film in a strong optical field can be understood from electron dynamics within a single conduction band. In the optical field, an electron with initial wave vector q is moving in the reciprocal space acquiring time-dependent wave vector $k_T(q, t)$ —see Eq. (6). Therefore all electrons are shifted in the reciprocal space by the same wave vector $\Delta q(t) = \frac{e}{\hbar} \int^t F_x(z, t_1) dt_1$, and the net current is generated. For a strong pulse, the shift, Δq , is large and, for $F_0 \gtrsim F_c$, can become

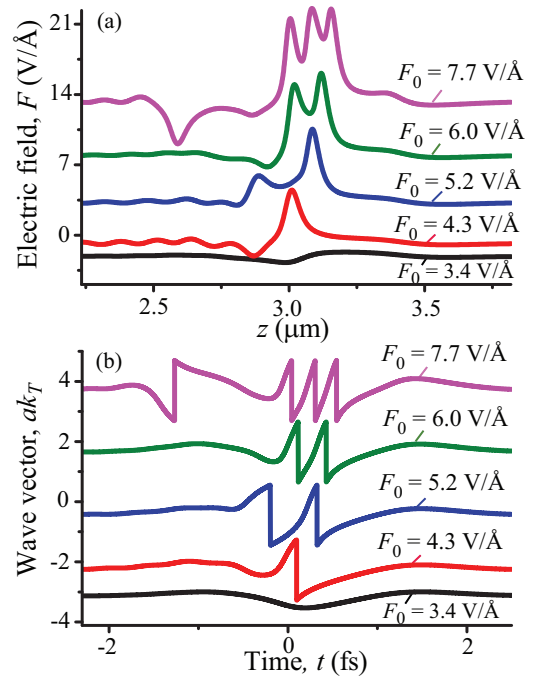


FIG. 4. (Color online) Bloch oscillations in the transmitted field and electron momentum. (a) Electric field distribution in space of the transmitted optical pulse is shown for different values of F_0 . (b) The corresponding dimensionless time-dependent wave vectors in the first Brillouin zone $ak_T(q = 0, t)$ as functions of time t . The origin of time is chosen arbitrary, and the graphs are offset vertically for clarity.

greater than the Brillouin zone extension $k = 2\pi/a$, causing the Bragg reflection of the electrons, which results in the Bloch oscillations and in the development of the WS localization.

At $F_0 \gtrsim F_c$, the electron current acquires oscillations at Bloch frequency $\omega_B \gtrsim 4\omega$, which suppresses the susceptibility at the optical frequency ω . This results in further loss of the metallic optical properties. Since the electron spectrum is discrete (the WS ladder) and, consequently, the density of states at the Fermi level is zero, the metal in strong optical fields behaves as a semimetal with a relatively high transparency and a low reflection coefficient. This is not fundamentally different from dielectrics in similar fields, cf. Refs. 10, 11, and 28, thus suggesting asymptotically universal behavior of solids in strong optical fields.

In Fig. 4(a), the spatial distribution of electric field in the transmitted optical pulse is shown for different values of amplitude F_0 . With increasing F_0 above the threshold, $F_c \approx 3.4$ V/Å, well pronounced Bloch oscillations develop in the field distribution. Their total number is proportional to field amplitude, $n \approx |e|aF_0/(2\hbar\omega)$. This is the number of times that an accelerated electron crosses the Brillouin zone boundary during quarter-period time $T/4$, as can be illustrated by comparison with the temporal dependence of the electron quasimomentum displayed in Fig. 4(b). These Bloch oscillations are also visible in the temporal evolution of electric field inside the metal film—cf. Fig. 2.

The highly nonlinear phenomena excited by strong and short pulses include a net transfer of charge, ΔQ , in the direction of the electric field of the pulse, which is a nonzero

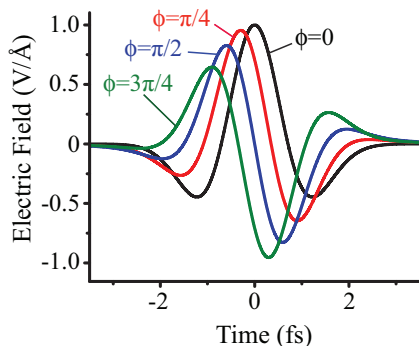


FIG. 5. (Color online) Excitation pulse waveforms $F_x(t, \phi)$ for $F_0 = 1 \text{ V/\AA}$ and four choices of the CEP, $\phi = 0, \pi/4, \pi/2, 3\pi/2$ (as indicated).

integral of current J_x ,

$$\Delta Q = \int_{-\infty}^{\infty} J_x(t) dt = P_x(t)|_{t=\infty} \Delta S, \quad (12)$$

where ΔS is the laser pulse cross section.

The metal fcc lattice is centrosymmetric, and the laser pulse-field area is zero. In this case, the direction of the charge transfer is determined by the carrier-envelope phase (CEP), ϕ , of the pulse, which defines the direction of the pulse-field maximum. The pulse of Eq. (1) possesses $\phi = 0$. We introduce a pulse with an arbitrary CEP using the Hilbert transform as

$$F_x(t, \phi) = F_x(t) \cos \phi + F_x^{(H)}(t) \sin \phi, \quad (13)$$

$$F_x^{(H)}(t) = \frac{1}{\pi} \mathcal{P} \int_{-\infty}^{\infty} \frac{F_x(t')}{t - t'} dt', \quad (14)$$

where $F_x^{(H)}(t)$ is the Hilbert transform of the pulse, see Eq. (1). Resulting pulses are displayed in Fig. 5 for $F_0 = 1 \text{ V/\AA}$ and four choices of the CEP, $\phi = 0, \pi/4, \pi/2, 3\pi/2$. Note that the pulse waveform is an even (symmetric) function for $\phi = 0$ and odd (antisymmetric) for $\phi = \pi/2$.

The transferred charge calculated from Eq. (12) is shown in Fig. 6 as a function of CEP ϕ of the pulse field, $F_x(t, \phi)$. The result illustrates that the charge transferred is nonzero despite the zero area of the pulse and the centrosymmetric lattice. Note that the charge transferred changes its sign when CPE is shifted by π , i.e., $\Delta Q(\phi + \pi) = -\Delta Q(\phi)$, which is due to a similar property of the pulse electric field, $F_x(t, \phi + \pi) = -F_x(t, \phi)$ [see Eq. (13)].

The direction of the charge transfer is correlated with the direction of the pulse-field maximum. For zero CEP, the pulse-field maximum in Fig. 5 is positive, i.e., pointing in the positive direction of the x axis, while the charge transferred is negative, see Fig. 6. Thus, the net charge is transferred in the direction *opposite* to the direction of the pulse-field maximum.

Such negative correlation between the direction of the strongest field and the direction of the charge transfer is due to the fact that the current generated by the pulse is suppressed at large electric fields, i.e., near the pulse maximum. This can be interpreted as the metal becoming less conductive,

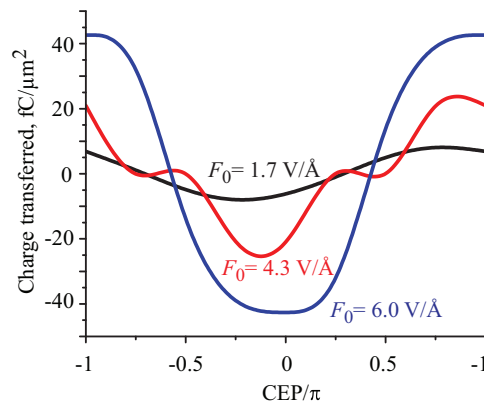


FIG. 6. (Color online) Charge transferred as a result of a single pulse as a function of the carrier-envelope phase (CEP) of the pulse. The results are shown for three pulse amplitudes F_0 as indicated in the figure using color coding.

semimetallic at high fields. Such behavior is diametrically opposite to that of dielectrics where charge is transferred in the direction of the maximum field, cf. Ref. 10. This is due to dielectrics becoming also semimetallic and, hence, more conductive in high fields.

IV. CONCLUSION

We have predicted a highly unusual and nontrivial behavior of metal nanofilms subjected to strong ultrashort (near-single oscillation) optical pulses with field amplitude $\gtrsim 4.3 \text{ V/\AA}$ (intensity $\gtrsim 5.0 \times 10^{14} \text{ W/cm}^2$). This includes such effects as disappearance of the metallic high reflection (suppression of the skin effect), a significant increase of transmission of the pulse energy through the nanofilm, while both the absorbance and the total energy deposition dramatically decrease at the high pulse intensity where the Bloch oscillations are pronounced. The optical field induces a transition to a semi-metal-like state, which is similar to that of dielectrics in correspondingly high fields. These phenomena develop at subcycle times $\lesssim 1 \text{ fs}$ and are driven by the field instantaneous strength. The transmitted and reflected pulses possess nonzero areas, which will cause net current (charge transfer) in media they affect. Note that the high intensities and short durations of the pulses required for the effects discussed in this article are within the reach of the existing generation methods.

ACKNOWLEDGMENTS

This work was supported by the Max Planck Society and the Deutsche Forschungsgemeinschaft Cluster of Excellence: Munich Center for Advanced Photonics (<http://www.munich-photonics.de>). Major funding was provided by Grant No. DE-FG02-01ER15213 from the Chemical Sciences, Biosciences and Geosciences Division. Supplementary funding came from Grant No. DE-FG02-11ER46789 from the Materials Sciences and Engineering Division of the Office of the Basic Energy Sciences, Office of Science, U.S. Department of Energy, and Grant No. ECCS-1308473 from NSF. We are grateful to Ferenc Krausz for useful discussions.

- ¹M. Lenzner, J. Kruger, S. Sartania, Z. Cheng, C. Spielmann, G. Mourou, W. Kautek, and F. Krausz, *Phys. Rev. Lett.* **80**, 4076 (1998).
- ²L. Miaja-Avila, C. Lei, M. Aeschlimann, J. L. Gland, M. M. Murnane, H. C. Kapteyn, and G. Saathoff, *Phys. Rev. Lett.* **97**, 113604 (2006).
- ³M. Gertsch, M. Spanner, D. M. Rayner, and P. B. Corkum, *J. Phys. B* **43**, 131002 (2010).
- ⁴A. V. Mitrofanov, A. J. Verhoef, E. E. Serebryannikov, J. Lumeau, L. Glebov, A. M. Zheltikov, and A. Baltuška, *Phys. Rev. Lett.* **106**, 147401 (2011).
- ⁵S. Ghimire, A. D. DiChiara, E. Sistrunk, P. Agostini, L. F. DiMauro, and D. A. Reis, *Nat. Phys.* **7**, 138 (2011).
- ⁶M. Durach, A. Rusina, M. F. Kling, and M. I. Stockman, *Phys. Rev. Lett.* **105**, 086803 (2010).
- ⁷M. Kruger, M. Schenk, and P. Hommelhoff, *Nature (London)* **475**, 78 (2011).
- ⁸S. Zherebtsov, T. Fennel, J. Plenge, E. Antonsson, I. Znakovskaya, A. Wirth, O. Herrwerth, F. Suessmann, C. Peltz, I. Ahmad *et al.*, *Nat. Phys.* **7**, 656 (2011).
- ⁹M. Durach, A. Rusina, M. F. Kling, and M. I. Stockman, *Phys. Rev. Lett.* **107**, 086602 (2011).
- ¹⁰A. Schiffrin, T. Paasch-Colberg, N. Karpowicz, V. Apalkov, D. Gerster, S. Muhlbrandt, M. Korbman, J. Reichert, M. Schultze, S. Holzner *et al.*, *Nature (London)* **493**, 70 (2012).
- ¹¹M. Schultze, E. M. Bothschafter, A. Sommer, S. Holzner, W. Schweinberger, M. Fiess, M. Hofstetter, R. Kienberger, V. Apalkov, V. S. Yakovlev *et al.*, *Nature (London)* **493**, 75 (2012).
- ¹²G. H. Wannier, *Elements of Solid State Theory* (Cambridge University Press, Cambridge, England, 1959).
- ¹³G. H. Wannier, *Phys. Rev.* **117**, 432 (1960).
- ¹⁴F. Bloch, *Z. Phys. A* **52**, 555 (1929).
- ¹⁵M. I. Stockman, *Opt. Express* **19**, 22029 (2011).
- ¹⁶E. E. Mendez and G. Bastard, *Phys. Today* **46**, 34 (1993).
- ¹⁷J. Feldmann, K. Leo, J. Shah, D. A. B. Miller, J. E. Cunningham, T. Meier, G. von Plessen, A. Schulze, P. Thomas, and S. Schmitt-Rink, *Phys. Rev. B* **46**, 7252 (1992).
- ¹⁸T. Dekorsy, P. Leisching, C. Waschke, K. Kohler, K. Leo, H. G. Roskos, and H. Kurz, *Semicond. Sci. Tech.* **9**, 1959 (1994).
- ¹⁹K. F. MacDonald, Z. L. Samson, M. I. Stockman, and N. I. Zheludev, *Nat. Phot.* **3**, 55 (2009).
- ²⁰K. S. Kunz and R. J. Luebbers, *The Finite Difference Time Domain Method for Electromagnetics* (CRC Press, Boca Raton, 1993).
- ²¹A. Taflov, *Computational Electrodynamics: The Finite-Difference Time-Domain Method* (Artech House, Boston, 2005).
- ²²J. C. Slater and G. F. Koster, *Phys. Rev.* **94**, 1498 (1954).
- ²³T. Frauenheim, G. Seifert, M. Elstner, Z. Hajnal, G. Jungnickel, D. Porezag, S. Suhai, and R. Scholz, *Phys. Status Solidi B* **217**, 41 (2000).
- ²⁴W. V. Houston, *Phys. Rev.* **57**, 184 (1940).
- ²⁵B. R. Cooper, H. Ehrenreich, and H. R. Philipp, *Phys. Rev.* **138**, A494 (1965).
- ²⁶R. R. Jones, D. You, and P. H. Bucksbaum, *Phys. Rev. Lett.* **70**, 1236 (1993).
- ²⁷C. Raman, C. W. S. Conover, C. I. Sukenik, and P. H. Bucksbaum, *Phys. Rev. Lett.* **76**, 2436 (1996).
- ²⁸V. Apalkov and M. I. Stockman, *Phys. Rev. B* **86**, 165118 (2012).